ACS OMEGA

Open Access

http://pubs.acs.org/journal/acsodf

Article

Green Synthesis of Gold Nanoparticles from Polygahatous Polysaccharides and Their Anticancer Effect on Hepatic Carcinoma through Immunoregulation

Maodong Leng, Huiqin Jiang, Sitong Zhang, and Yixi Bao*

Cite This: *ACS Omega* 2024, 9, 21144−21151

Read Online

ACCESS | Metrics & More | Article Recommendations

ABSTRACT: Hepatic carcinoma is one of the leading causes of morbidity and mortality among all cancers, but no effective treatment measures have been developed. Herein, polystyrene polysaccharide (PSP) extracted from *Polygonatum* was used to synthesize gold nanoparticles (PSP-AuNPs) by heating and reduction methods, and the characteristics of the PSP-AuNPs were detected after successful synthesis. *In vitro*, the immunoregulatory effects of PSP-AuNPs were studied by testing the concentrations of NO, TNF-α, and IL-12p70 in the culture media of PSP-AuNPs-treated RAW264.7 macrophages, and the effect of biocompatibility on the viability of RAW264.7 macrophages and L02 cells was studied *via* a CCK-8 assay. *In vivo*, tumor-bearing mice were established and treated with PSP-AuNPs, and the anticancer effects were studied by detecting trends in tumor volume, tumor inhibition rate, and tumor cell proliferation index. Immunoregulation was assessed by evaluating the serum levels of TNF-α and IL-10, the CD4+/CD8+ lymphocyte ratio in peripheral blood and the spleen and thymus indices; toxicity was investigated by measuring body weight, liver and renal function indices. The results showed that PSP-AuNPs could regulate immune function both *in vitro* and *in vivo* with almost no toxicity. PSP-AuNPs exhibited excellent anticancer effects on hepatic carcinoma *in vivo*. The anticancer effect could be strengthened, and the toxicity could be reduced by the combined use of PSP-AuNPs and ADM. In conclusion, PSP-AuNPs could be effective as a therapy and adjuvant therapy for treating hepatic carcinoma, providing potential treatment strategies for this disease.

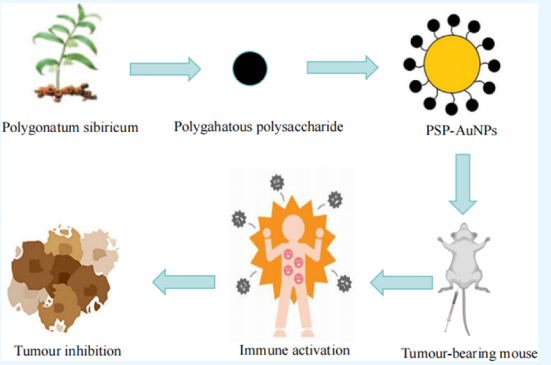

1. INTRODUCTION

Hepatic carcinoma is one of the most common cancers worldwide, with morbidity and mortality rates ranking sixth and third respectively among all cancers.[1] The incidence of hepatic cancer remains stable among men, but obesity and hepatitis B and C virus infections have contributed to the stable increase in incidence among women (1.6−1.7% annually).[2] Current therapeutic methods for treating hepatic carcinoma include surgery, targeted treatment, and immunotherapy, but these methods are restricted for use due to several limitations. Surgery is an effective treatment method for hepatic carcinoma, but it is not suitable for the majority of patients because of the usually advanced stages of hepatic carcinoma at diagnosis.[3] Targeted treatment with sorafenib has achieved significant effect in the systemic treatment, but it can be ineffective due to the abnormal heterogeneity of hepatic carcinoma and rapid development of drug resistance, and the 3-month survival rate is still low.[4−6] Immune checkpoint inhibitors such as nivolumab, altizolizumab, and bevacizumab are used for immunotherapy of hepatic carcinoma, and relatively good effects, including prolonged overall survival (OS) and progression-free survival (PFS), can be obtained.[7−10] However, the effects of immunotherapy are still limited, and hepatic carcinoma is prone to recurrence and distant metastasis. In addition, targeted therapy and immunotherapy in hepatic carcinoma could cause various adverse effects such as gastrointestinal toxicity, hepatotoxicity, and endocrine-related toxicity. Therefore, there is an urgent need to develop new treatments for hepatic carcinoma.

Traditional Chinese medicine (TCM) can be used as an adjuvant therapy for radiation and chemotherapy to strengthen therapeutic effects and reduce adverse effects.[11,12] Components, including polysaccharides, phenolic acids, flavonoids, esters, and cumarin, can be purified from TCMs *via* modern purification methods.[13] Polysaccharides purified from TCMs can enhance immunity without causing toxicity during cancer therapy.[14,15] *Polygonatum* is the dry rhizoma of the plant

Received: January 31, 2024
Revised: March 19, 2024
Accepted: April 24, 2024
Published: May 2, 2024

Polygonatum sibiricum. Polygahatous polysaccharide (PSP) is extracted from *Polygonatum* and has various biological functions, including immunoregulation, antioxidant activity, reducing diabetes complications, preventing osteoporosis, and exerting antitumor effects.[16−20] However, the immunoregulatory function and anticancer effect of PSP on hepatic carcinoma are unknown.

In recent years, an increasing number of nanomaterials have been studied for the treatment of hepatic carcinoma, and these materials can deliver small molecular substances such as chemotherapeutics, polysaccharides, and therapeutic agents; increase dispersion, solubility, and stability; and change pharmacokinetics.[21−23] Uptake of the anticancer cargo inside the cells remains a major challenge in the application of nanomaterials; membrane potential and receptor-mediated uptake of nanoparticles are important factors, and receptor-mediated approach has been confirmed as a useful method to increase the uptake of nanomaterial drugs inside hepatic cancer cells.[24,25] Gold nanoparticles (AuNPs) are the most widely studied type of nanoparticle, and they can be easily combined with drugs and increase the stability of drugs due to their optical, plasmon resonance, and biological conjugation properties.[26] AuNPs possess advantages, including low toxicity, slowing drug degradation, and reducing the dosage and toxicity of drugs used.[27] AuNPs have been widely used in biomedical fields, including clinical chemistry, immunology, microbiology, the diagnosis, and treatment of malignant tumors.[28,29] Previous studies have demonstrated that the effects of the combination of AuNPs with extracts and polysaccharides from TCM are superior to the effects of single TCM ingredients in the treatment of liver cancer.[30,31] The most common method for synthesizing AuNPs involves the reduction of dissolving gold salt, such as chloroauric acid. Therefore, AuNPs might be synthesized through the reduction of chloroauric acid with PSP (PSP-AuNPs), reducing the toxicity of drugs and extending the duration of drug circulation to achieve more efficient biological functions.

In this study, we will synthesize PSP-AuNPs *via* a green method and investigate the role of these nanoparticles in the treatment and adjuvant treatment of hepatic carcinoma through immunoregulation. In contrast to the earlier approaches for hepatic carcinoma treatments, this study will provide a new strategy for therapy. The new method for hepatic carcinoma therapy will increase the uptake of drugs in cells due to the use of AuNPs, reduce the adverse effects caused by targeted and immune inhibitor chemotherapy, and provide an alternative therapy method for patients at advanced stages who lose the opportunity of surgery.

2. MATERIALS AND METHODS

2.1. Synthesis of PSP-AuNPs. The PSP powder used in this study was purchased from Sichuan Weikeqi Biological Technology Company (Chengdu, China) and had purity greater than 90% and was free of endotoxin. PSP-AuNPs were synthesized with the use of PSP and HAuCl4 (1 M) under heating conditions. To obtain the optimal conditions for the synthesis, we continuously changed the following reaction conditions: concentration of PSP (10 mg/mL-0.5 mg/mL); reaction volume (0.5 mL-5 mL); amount of $HAuCl_4$ (3 μL, 2.5 μL, 2 μL, 1.5 μL, 1.25 μL, 1 μL, 0.5 μL, 0.2 μL); reaction time (10 min, 15 min, 30 min, 45 min); and reaction temperature (60 °C, 80 °C, 100 °C). When the color of the solution changed from light yellow to ruby red, the synthesis of PSP-AuNPs was preliminarily considered successful[26] and further tests were performed to analyze the synthesis and characterization of the nanoparticles. In addition, sodium citrate dihydrate and HAuCl4 (1 M) were used to synthesize AuNPs as controls.[32]

2.2. Characterization of PSP-AuNPs. The ultraviolet−visible absorption spectrum (UV−VIS, range: 200−800 nm) was used to detect the PSP, PSP-AuNP, and AuNP solutions to confirm the success of the synthesis and analyze the absorption peak. Transmission electron microscopy (TEM) and atomic force microscopy (AFM) were used for the detection of the size and morphological characteristics (TEM for the overall shape and AFM for the surface morphology) of PSP-AuNPs and AuNPs, Fourier transform infrared spectroscopy (FTIR) was used to analyze the functional groups of PSP-AuNPs, dynamic light scattering (DLS) was used to detect the size and zeta distributions of PSP-AuNPs, and energy dispersive X-ray (EDX) was used to characterize the energy spectrum of PSP-AuNPs.

2.3. Cell Culture. RAW264.7 macrophages were donated by the Clinical Laboratory Department of the Second Affiliated Hospital of Chongqing Medical University. To prevent differentiation, RAW264.7 macrophages were cultured in specialized complete DMEM (Procell, Wuhan, China). We obtained H22 cells from Procell, and RPMI-1640 culture medium supplemented with 10% fetal bovine serum (FBS) was used for culture. RPMI-1640 supplemented with 20% FBS was used to culture L02 cells (Cellverse Bioscience, Shanghai, China). All the culture media were supplemented with 1% penicillin and streptomycin. The culture conditions for the three cell lines in the cell incubator were 5% CO_2 and 37 °C.

2.4. Tests of NO, TNF-α, and IL-12p70 Levels. The *in vitro* immunoregulatory function of PSP-AuNPs was investigated in RAW264.7 cells. Equal amounts of RAW264.7 cells (5×10^4 cells/well) were seeded in each well of 24-well plates. After 24 h of adhesion and adaptation, the RAW264.7 cells were treated with LPS (100 ng/mL; ACMEC, China), different concentrations of PSP and PSP-AuNPs (100−500 μg/mL) separately. Cells not treated (normal control group, NC) and treated with LPS were regarded as negative and positive controls, respectively. The supernatants were collected and centrifuged for immunoregulation tests after 24 h of treatment. The Griess reaction was used to detect NO levels, and the levels of TNF-α and IL-12p70 were detected *via* ELISA. The tests were performed with a Micro Nitric Oxide (NO) Assay Kit (Abbkine, USA) and an ELISA Kit (Elabscience, Wuhan, China) according to the manufacturers' instructions.

2.5. CCK-8 Assay. RAW264.7 macrophages and L02 cells were plated on 96-well plates with equal amounts of cells in each well (5×10^3 cells/well). After 24 h of incubation, both cell lines were treated with different concentrations of PSP and PSP-AuNPs (100−500 μg/mL). In addition, RAW264.7 macrophages and L02 cells were treated with LPS (100 ng/mL) and adriamycin (ADM) (2 μg/mL; HARVEYBIO, China), respectively, as controls. Normal controls without any treatment (NC) were used for both cell lines. After 24 h of treatment, 10 μL of CCK-8 solution (Biosharp Life Sciences, China) was added to each well. The plates were incubated for more than 1.5 h to react before the absorbance was measured at 450 nm with an ELISA instrument. The following formula was used for the calculation of cell viability: cell viability (%) =

https://doi.org/10.1021/acsomega.4c01025
ACS Omega 2024, 9, 21144−21151

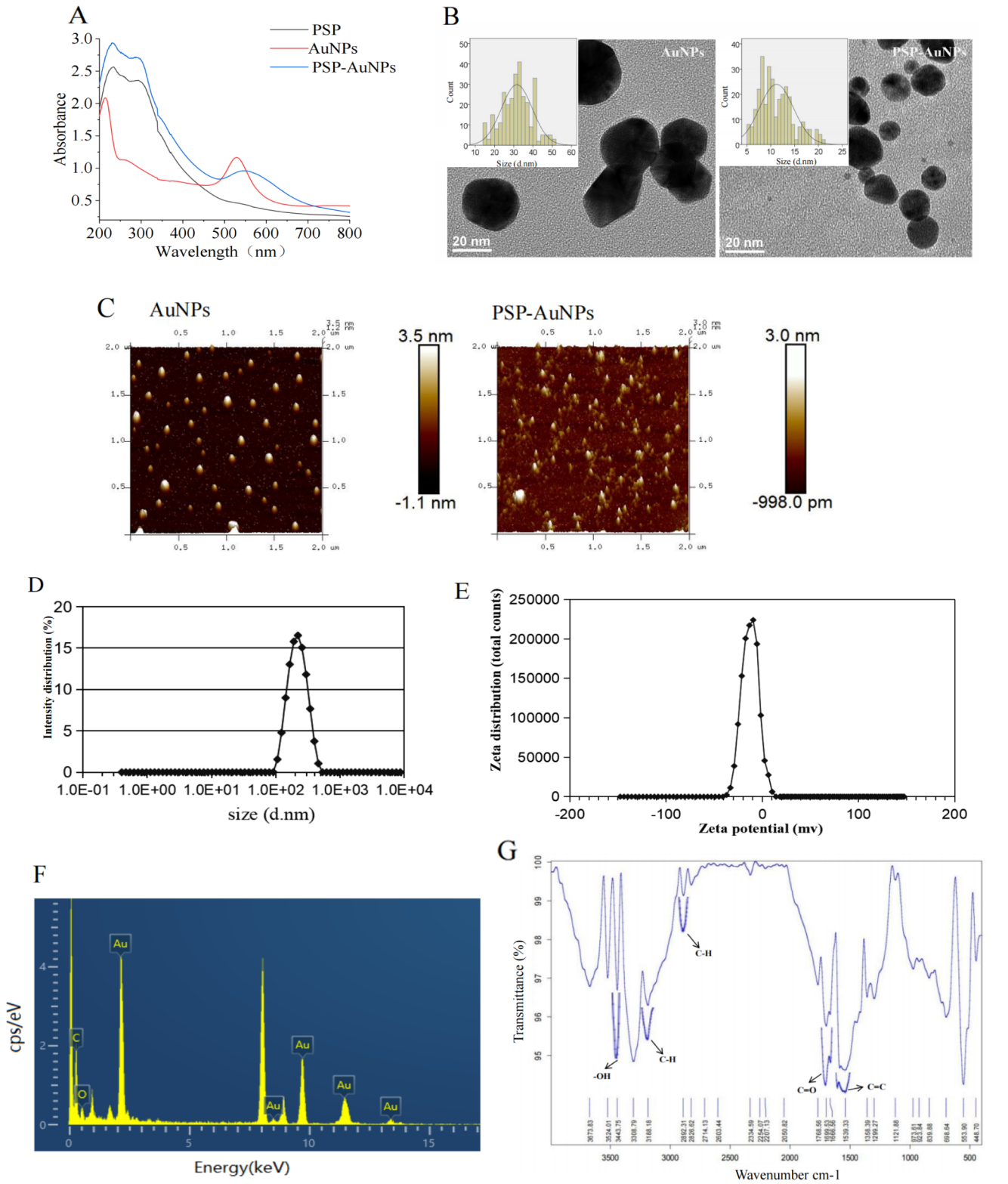

Figure 1. Characteristics of PSP-AuNPs. (A) UV−VIS images of PSP, AuNPs, and PSP-AuNPs. (B) TEM images of AuNPs and PSP-AuNPs. (C) AFM images of AuNPs and PSP-AuNPs. (D) Size and (E) zeta distributions determined by DLS. (F) EDX analysis. (G) FTIR results.

[OD (experiment) − OD (blank)]/[OD (NC) − OD (blank)] × 100%.

2.6. Animals. We purchased female C57BL/6 mice from the Laboratory Animal Center of Zhengzhou University. The weights of the mice were 16−18 g, and the mice were approximately 6 weeks old. Hepatic carcinoma tumor-bearing mice model was established through injecting H22 cells (4×10^5) into the subcutaneous right axilla of the mice. The tumor-bearing mice were randomly assigned to one of the following groups: (1) normal saline (NS) (400 μL/mouse/day), (2) PSP (200 mg/kg/day), (3) PSP-AuNPs (200 mg/kg/day), (4) ADM (4 mg/kg/3 days), and (5) PSP-AuNPs + ADM. Five

https://doi.org/10.1021/acsomega.4c01025
ACS Omega 2024, 9, 21144−21151

mice were included in each group, and the drugs were administered *via* intraperitoneal injection.

During administration, the body weights of the mice and the diameters of the tumors were measured with a laboratory balance and a Vernier caliper every 3 days. The longest (a) and shortest (b) diameters of the tumors were obtained, and $a \times b^2/2$ was used to calculate the tumor volume.[33] Moreover, the activities and mental states of the mice were recorded. The mice were administered with these agents for 21 days, then the mice were sacrificed by cervical dislocation. Peripheral blood was collected from the mice into heparin lithium-anticoagulant tubes for flow cytometry (FCM) analysis and procoagulant separation tubes for the separation of serum. After centrifugation, the serum was subjected to ELISA and biochemical tests. The weights of the tumors, spleens, and thymuses were recorded after isolation. The tumor inhibition rate was calculated as $(1 - a/b) \times 100\%$ (a indicates the weights of the tumors in the experimental groups; b represents the weights in the NS group). The spleen and thymus indices of the mice were calculated with the following formula: Organ index = spleen (thymus) weight/body weight ×100%. Polyoxymethylene (4%) was used to preserve the tumors for immunohistochemical tests.

2.7. ELISA and Biochemical Tests. The serum levels of TNF-α and IL-10 in tumor-bearing mice were detected with ELISA kits (Elabscience, Wuhan, China) according to the manufacturer's instructions. Biochemical analysis was performed with the use of a fully automatic biochemical analyzer (HITACHI, Japan). Qualified operations were performed to test the levels of liver (alanine aminotransferase [ALT] and aspartic transaminase [AST]) and renal (creatinine [CREA] and blood urea [UREA]) function indices.

2.8. FCM Analysis. FCM analysis was performed for the tests of CD3, CD4, and CD8 positive cells, and the whole blood was mixed with the corresponding antibodies at the proper proportions. The CD3 antibody was labeled with FITC, the CD4 antibody was labeled with PE, and the CD8 antibody was labeled with APC. The mixture was kept in the dark for 20 min at room temperature. Lysing buffer (BD Biosciences, USA) was used to lyse red blood cells, and the reaction was completed at 37 °C for 20 min. After three washes with PBS (×200 g, 5 min), the cells were suspended in PBS for FCM analysis. A BD Accuri^{FM} C6 Plus Flow Cytometer was used for FCM analysis.

2.9. Immunohistochemical Analysis. Paraffinized tumor sections were generated from the tumor tissues. Proliferation cell nuclear antigen (PCNA) staining was performed with the following procedure: dewaxing, antigen retrieval, blocking endogenous peroxidase, nonspecific binding blocking, primary PCNA antibody (Servicebio, China), incubation (4 °C, overnight), and secondary antibody incubation (50 min, room temperature). 3DHISTECH was used to visualize the sections stained with diaminobenzidine (DAB), and three random fields (400× magnification) from each image were obtained. The proliferation index was calculated as the ratio of PCNA-positive cells to total cells.

2.10. Statistical Analysis. The average value and variation in the quantitative data are expressed as the mean ± standard deviation (SD). One-way analysis of variance (ANOVA) was performed when the data were compared among more than two groups, and differences between two groups were further analyzed with Student−Newman−Keuls multiple comparison tests. Student's t test was used for comparisons between two groups. $p < 0.05$ was considered to indicate statistical significance. All the statistical analyses were performed with IBM SPSS Statistics 21.

3. RESULTS

3.1. Characteristics of PSP-AuNPs. The optical conditions for the synthesis of PSP-AuNPs were as follows: 1 mg/mL PSP in a 3.5 mL reaction mixture with 0.5 μL of HAuCl4 solution (1 M) were reacted at 80 °C for 15 min. From the UV−VIS results (Figure 1A), the characteristic absorption peak of PSP-AuNPs is between 540 and 550 nm, which is near the absorption peak of AuNPs. The TEM (Figure 1B) and AFM images (Figure 1C) demonstrated the successful synthesis of PSP-AuNPs, and the overall shape and surface morphology of PSP-AuNPs were different from those of AuNPs. The size (Figure 1D) and zeta (Figure 1E) distributions of the PSP-AuNPs determined by DLS were similar to normal distribution. The sizes of the PSP-AuNPs were mainly between 91 and 459 nm, and the zeta potentials were ranged from −35 to 10 mV. According to the EDX results, the percentages of C, O, and Au are 74.70%, 7.78%, and 17.52%, respectively. According to the FTIR analysis, the absorption peaks at 1699.53 cm^{-1}, 3443.75, and 1539.33 cm^{-1} were ascribed to the stretching vibrations of C═O, −OH, and C═C, respectively. The stretching vibration of C−H accounted for the absorption peaks at 3188.18 and 2892.31 cm^{-1}.

3.2. Concentrations of NO, TNF-α, and IL-12p70 in the Culture Media of RAW264.7 Cells. As demonstrated (Figure 2), the concentrations of NO (Figure 2A), TNF-α (Figure 2B), and IL-12p70 (Figure 2C) in the culture media of RAW264.7 cells stimulated with PSP and PSP-AuNPs were greater than those in the NC group and lower than those in the LPS group. The concentrations of NO, TNF-α, and IL-12p70 in the culture media of the PSP-AuNPs were greater than those in the PSP group at stimulation concentrations from 200 to 500 μg/mL. The concentrations of NO, TNF-α, and IL-12p70 reached their highest values at 400 μg/mL for PSP and 300 or 400 μg/mL for PSP-AuNPs.

3.3. The Viability of RAW264.7 and L02 Cells Treated with PSP-AuNPs. The viability of RAW264.7 cells (Figure 3A) was greater in the PSP and PSP-AuNP groups than in the NC group and lower than that in the LPS group, and the viability in the PSP-AuNP group was greater than that in the PSP group at concentrations from 200 to 500 μg/mL. The viability of L02 cells (Figure 3B) treated with PSP and PSP-AuNPs was greater than that of the ADM and NC groups, and the viability of the PSP-AuNP group was greater than that of the PSP group at all treated concentrations.

3.4. Biocompatibility and Toxicity of PSP-AuNPs *In Vivo*. The body weights of the mice in the PSP, PSP-AuNPs, and NS groups were increased with time and were decreased in the ADM and PSP-AuNPs+ADM groups (Figure 4A). The body weights of the PSP group were greater than those of the NS group and lower than those of the PSP-AuNP group. The body weights of the PSP-AuNPs + ADM group were greater than those of the ADM group and lower than those of the NS group. The serum levels of ALT, AST (Figure 4B), CREA, and UREA (Figure 4C) were lower in the PSP and PSP-AuNP groups than those in the NS group. Liver and renal function indices were lower in the PSP-AuNP group than those in the PSP group. The liver and renal function indices were lower in the PSP-AuNPs + ADM group than those in the ADM group.

https://doi.org/10.1021/acsomega.4c01025
ACS Omega 2024, 9, 21144−21151

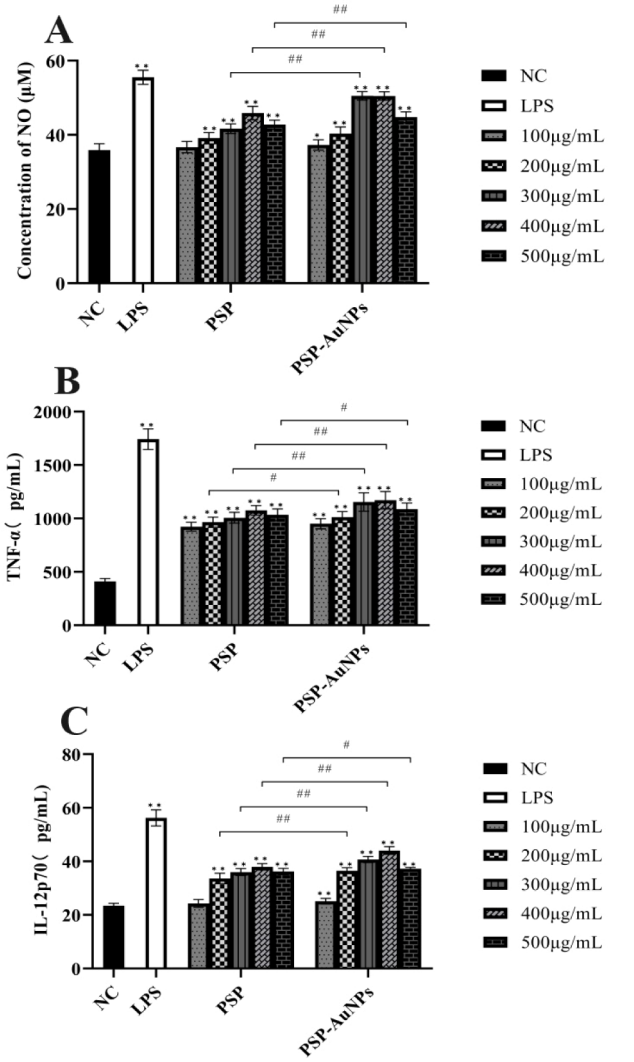

Figure 2. Concentrations of NO (A), TNF-α (B), and IL-12p70 (C) in the culture medium of RAW264.7 cells. *p < 0.05, **p < 0.01, compared with the NC group; #P < 0.05, ##P < 0.01, compared with the PSP group.

In addition, PSP-AuNPs increased the activities of the mice in the PSP-AuNPs and PSP-AuNPs + ADM groups.

3.5. Immunoregulation of PSP-AuNPs *In Vivo*. The spleen (Figure 5A) and thymus (Figure 5B) indices, serum TNF-α levels (Figure 5C), and CD4+/CD8+ lymphocyte ratio (Figure 5E) were greater, and the serum IL-10 level (Figure 5D) was lower in the PSP-AuNP group than in the NS and PSP groups. Similarly, compared with those in the ADM group, the spleen and thymus indices, serum TNF-α levels, and CD4+/CD8+ lymphocyte ratio were greater, and the serum IL-10 concentration was lower in the PSP-AuNPs + ADM group.

3.6. Antitumor Effects of PSP-AuNPs. The PSP-AuNP group demonstrated a greater tumor inhibition rate (Figure 6B), slower tumor growth (Figure 6C), and lower proliferation index (Figure 6D) than the PSP and NS groups did. The tumor inhibition rate was greater, tumor growth was slower, and the proliferation index was lower in the PSP-AuNPs + ADM group than those in the ADM group.

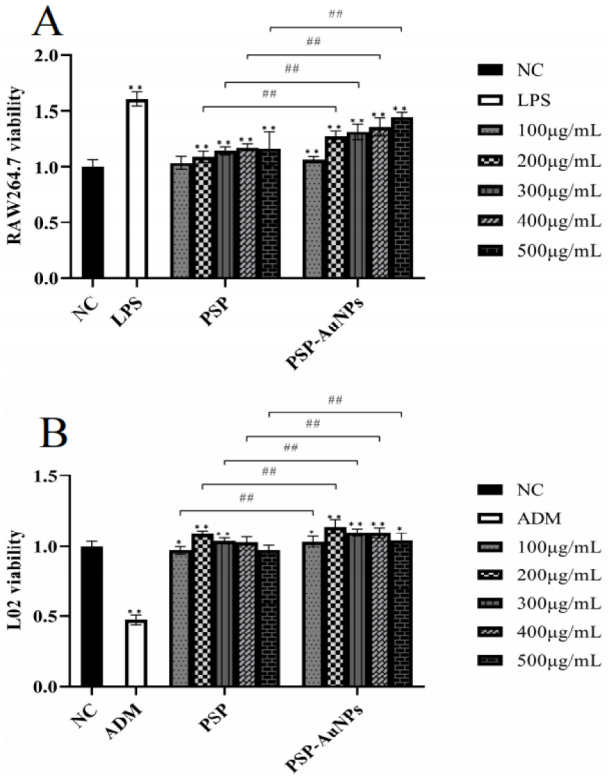

Figure 3. Viability of RAW264.7 (A) and L02 cells (B). *p < 0.05, **p < 0.01, compared with the NC group; #P < 0.05, ##P < 0.01, compared with the PSP group.

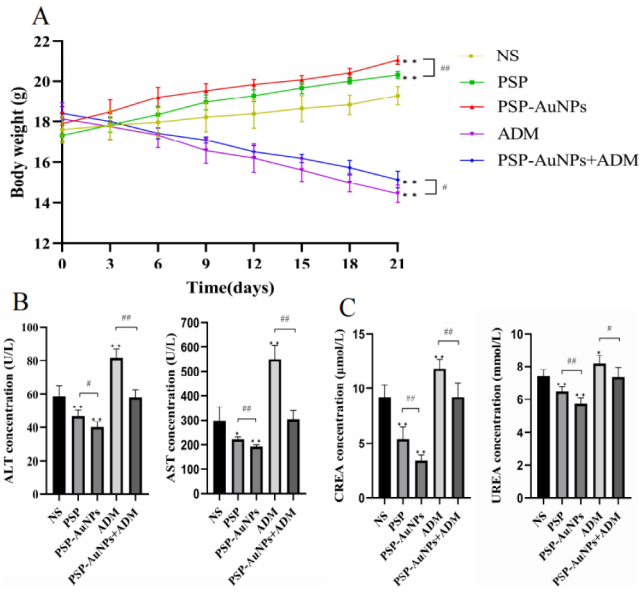

Figure 4. Biocompatibility and toxicity of PSP-AuNPs in hepatic carcinoma tumor-bearing mice. (A) The trends in body weight. (B) The serum levels of liver function indices (ALT and AST). (C) The serum levels of renal function indices (CREA and UREA). *p < 0.05, **p < 0.01, compared with the NS group; #P < 0.05, ##P < 0.01, compared with the PSP or ADM group.

4. DISCUSSION

In this study, we adopted a green method to synthesize gold nanoparticles from PSP to reduce the toxicity and increase the function of PSP. The results of the *in vitro* and *in vivo*

https://doi.org/10.1021/acsomega.4c01025
ACS Omega 2024, 9, 21144−21151

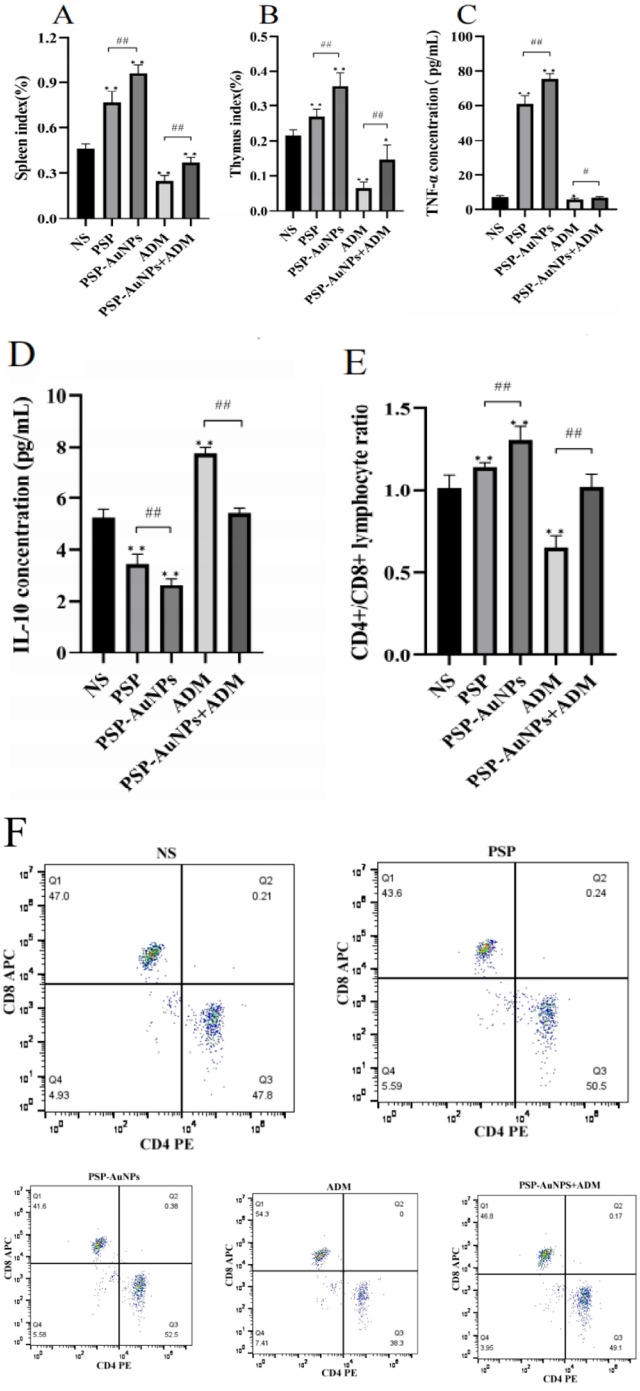

Figure 5. Immunoregulation of PSP-AuNPs *in vivo*. (A) Spleen index. (B) Thymus index. (C) Serum TNF-α concentration. (D) IL-10 concentration. (E) CD4+/CD8+ lymphocyte ratio. (F) FCM analysis of CD4+ and CD8+ lymphocytes.

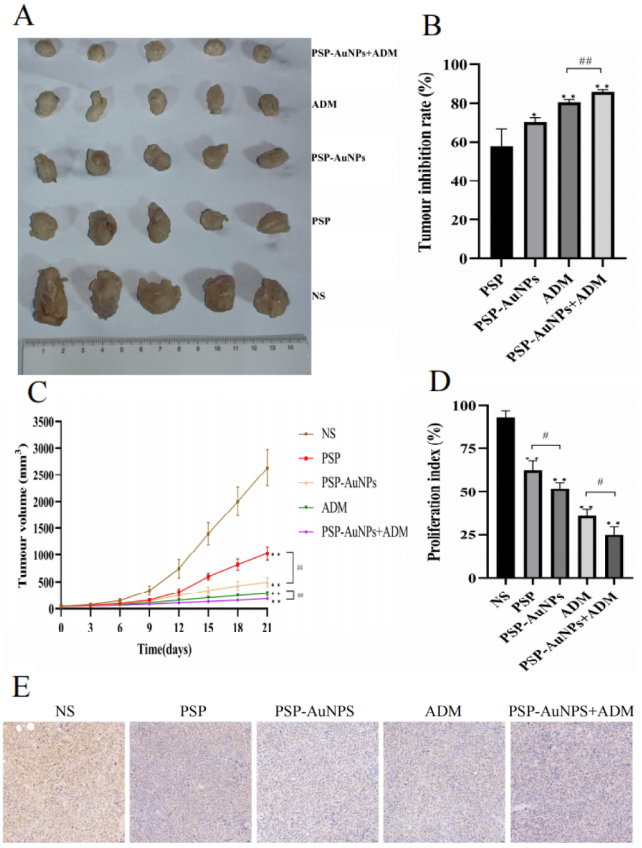

Figure 6. Antitumor effect of PSP-AuNPs. (A) Images of the isolated tumors. (B) Tumor inhibition rate. (C) Growth trends of tumor volumes. (D) Proliferation indices of tumor cells. (E) Images of PCNA staining (×400).

experiments revealed that, compared with PSP, PSP-AuNPs could increase immunoregulation, anticancer effects, and biocompatibility.

The successful synthesis of PSP-AuNPs was primarily identified by the color change of the reaction solution from yellow to ruby red, then confirmed by the UV−VIS, TEM, AFM, DLS, EDX, and FTIR results. The sizes of PSP-AuNPs determined by TEM were smaller than those of AuNPs, whereas the characteristic absorption peak of AuNPs was lower than that of PSP-AuNPs, which might be attributed to the different syntheses process between PSP-AuNPs and AuNPs. The AFM results showed that the surface morphology of PSP-AuNPs were more irregular than that of AuNPs, which might be due to the combination of PSP in PSP-AuNPs. The sizes of PSP-AuNPs tested by DLS were larger than those tested by TEM, which might be due to the different degree of dispersion of PSP-AuNPs in the solution and the difference between these two kinds of test methods. Nanoparticles with sizes larger than 6−8 nm and negatively charged can be prevented from filtration by the kidneys.[27,34] Form the DLS results, the sizes of the PSP-AuNPs were large enough, and the zeta potentials were mostly negative, which prevented filtration by the kidneys and allowed the accumulation of PSP-AuNPs in the liver. The EDX results demonstrated the presence of C, O, and Au in the PSP-AuNPs, and the percentages of C and O in PSP-AuNPs were very high, demonstrating the large amounts of PSP combined to AuNPs. The functional groups of C═O, −OH, C═C, and C−H identified by FTIR suggested the endogenous reducibility of PSP[35] which laid the foundations of PSP-AuNPs function.

PSP-AuNPs demonstrated greater biocompatibility than PSP did: *in vitro*, the viabilities of RAW264.7 macrophages and L02 cells treated with PSP-AuNPs were greater than those treated with PSP; and *in vivo*, tumor-bearing mice treated with PSP-AuNPs had greater body weights, greater activity, and lower liver function (ALT and AST) and renal function (CREA and UREA) indices. Therefore, PSP-AuNPs could be safer than PSP for drug use. Immunoregulatory function of PSP-AuNPs *in vitro* was evaluated by testing the levels of

https://doi.org/10.1021/acsomega.4c01025
ACS Omega 2024, 9, 21144−21151

immunoregulation factors including NO, TNF-α, and IL-12p70 secreted by RAW264.7 cells. The serum levels of TNF-α and IL-10, CD4+/CD8+ T lymphocyte ratio showed by FCM analysis, and spleen and thymus indices were tested to demonstrate the *in vivo* immunoregulatory function of PSP-AuNPs. NO might be considered as a potential therapeutic agent for cancer because it can regulate immunity through the activation of T lymphocytes.[36,37] TNF-α functions in innate immunity and the lymphocyte-mediated adaptive immune response, and high-dose local administration of TNF-α results in powerful tumor necrosis.[38,39] IL-12p70 originates from monocytes, and systemic administration of IL-12p70 has been demonstrated to have antitumor effects on various preclinical animal models as well as modest activity in cancer patients.[40] IL-10 is secreted mainly by macrophages, and this cytokine can induce immunosuppression and tumor progression.[41] Increased expression of IL-10 is correlated with poorer prognosis in several viral-correlated malignancies.[42] The CD4+/CD8+ T lymphocyte ratio is often used to evaluate immune system function, and an increased ratio can predict a favorable treatment response.[43] PSP-AuNPs exhibited greater immunoregulatory effects than PSP *in vitro* because of the greater expression levels of NO, TNF-α, and IL-12p70 in the culture medium of RAW264.7 macrophages treated with PSP-AuNPs. *In vivo*, the serum TNF-α concentration, CD4+/CD8+ T lymphocyte ratio, and spleen and thymus indices were greater, and the serum IL-10 concentration was lower in the PSP-AuNPs group than those in the PSP group, suggesting that the immunoregulation of PSP-AuNPs was greater. The biocompatibility and immunoregulation functions of PSP-AuNPs and PSP were tested on different concentrations to determine the appropriate concentrations of PSP-AuNPs for use. According to the study by Long T et al., PSP exerts tumor inhibitory effects through immunoregulation.[44] The hepatic carcinoma tumor volumes grew more slowly, the tumor inhibition rate was greater, and the tumor cell proliferation rate demonstrated by PCNA staining of the tumor sections was lower in the PSP-AuNPs-treated group than those in the PSP group. Therefore, PSP-AuNPs demonstrated greater hepatic carcinoma tumor inhibition effect through immunoregulation than PSP did. In contrast to previous studies,[30,45] we synthesized PSP-AuNPs from PSP with high a purity (>90%), and this strength facilitated studying the particular immunoregulation and anticancer function of PSP-AuNPs. We not only synthesized the nanoparticles successfully but also confirmed the anticancer effect on hepatic carcinoma of PSP-AuNPs through immunoregulation.

Interestingly, the tumor inhibition effect was greater in the PSP-AuNPs + ADM group than that in the ADM and PSP-AuNPs groups. In contrast to the destruction of immunoregulation, liver and renal functions caused by ADM, the combined use of PSP-AuNPs and ADM could help reverse some of those functions and protect the organs. As a result, the combined use of PSP-AuNPs and ADM could strengthen the anticancer effects of ADM and reduce the adverse effects.

5. CONCLUSIONS

The synthesis of PSP-AuNPs *via* a green method could increase the tumor inhibition effect of PSP in the treatment of hepatic carcinoma through enhancing immunoregulation. The combined use of PSP-AuNPs could reduce the adverse effects caused by chemotherapy and strengthen the anticancer effects. Our study has provided potential strategies for the future treatment of hepatic carcinoma.

■ ASSOCIATED CONTENT

Data Availability Statement

The data underlying the article are available throughout the manuscript and supporting files.

■ AUTHOR INFORMATION

Corresponding Author

Yixi Bao − *Department of Clinical Laboratory, The Second Affiliated Hospital of Chongqing Medical University, Chongqing 400010, China*; Phone: 0086-023-63693138; Email: yixibao@cqmu.edu.cn; Fax: 0086-023-63693138

Authors

Maodong Leng − *Department of Clinical Laboratory, The Second Affiliated Hospital of Chongqing Medical University, Chongqing 400010, China; Department of Clinical Laboratory, Zhengzhou Key Laboratory of Children's Infection and Immunity, Children's Hospital Affiliated to Zhengzhou University, Zhengzhou, Henan 450018, China*; orcid.org/0000-0002-1024-3706

Huiqin Jiang − *Innovation Center of Basic Research for Metabolic-Associated Fatty Liver Disease, Ministry of Education of China, Tianjian Laboratory of Advanced Biomedical Sciences, Institute of Advanced Biomedical Sciences, Zhengzhou University, Zhengzhou, Henan 450000, China*

Sitong Zhang − *Department of Clinical Laboratory, The Second Affiliated Hospital of Chongqing Medical University, Chongqing 400010, China*; orcid.org/0009-0007-7203-1817

Complete contact information is available at: https://pubs.acs.org/10.1021/acsomega.4c01025

Funding

This work was supported by Tianjian Laboratory of Advanced Biomedical Sciences.

Notes

The authors declare no competing financial interest.

■ ACKNOWLEDGMENTS

The authors thank the Pediatric Medical Research Institute of Children's Hospital Affiliated to Zhengzhou University and Academy of Medical Sciences of Zhengzhou University for providing laboratories and instruments to perform the experiments.

■ REFERENCES

(1) Zheng, S.; Bian, H.; Li, J.; Shen, Y.; Yang, Y.; Hu, W. Differentiation therapy: Unlocking phenotypic plasticity of hepatocellular carcinoma. *Crit. Rev. Oncol. Hematol.* **2022**, *180*, 103854.

(2) Siegel, R. L.; Miller, K. D.; Wagle, N. S.; Jemal, A. Cancer statistics, 2023. *Ca-Cancer J. Clin.* **2023**, *73* (1), 17−48.

(3) Forner, A.; Reig, M.; Bruix, J. Hepatocellular carcinoma. *Lancet* **2018**, *391* (10127), 1301−1314.

(4) El-Serag, H. B.; Marrero, J. A.; Rudolph, L.; Reddy, K. R. Diagnosis and treatment of hepatocellular carcinoma. *Gastroenterology* **2008**, *134* (6), 1752−1763.

(5) Keating, G. M. Sorafenib: A Review in Hepatocellular Carcinoma. *Target Oncol.* **2017**, *12* (2), 243−253.

(6) Fu, J.; Wang, H. Precision diagnosis and treatment of liver cancer in China. *Cancer Lett.* **2018**, *412*, 283−288.
(7) Kong, F. H.; Ye, Q. F.; Miao, X. Y.; et al. Current status of sorafenib nanoparticle delivery systems in the treatment of hepatocellular carcinoma. *Theranostics* **2021**, *11* (11), 5464−5490.
(8) Yang, X. A.; Jin, R.; Zhang, L. M.; Ying, D. J. Global trends of targeted therapy for hepatocellular carcinoma: A bibliometric and visualized study from 2008 to 2022. *Medicine* **2023**, *102* (34), No. e34932.
(9) Demir, T.; Lee, S. S.; Kaseb, A. O. Systemic therapy of liver cancer. *Adv. Cancer Res.* **2021**, *149*, 257−294.
(10) Lee, M. S.; Ryoo, B. Y.; Hsu, C. H.; et al. Atezolizumab with or without bevacizumab in unresectable hepatocellular carcinoma (GO30140): An open-label, multicentre, phase 1b study. *Lancet Oncol.* **2020**, *21* (6), 808−820.
(11) Xue, T. Synergy in traditional Chinese medicine. *Lancet Oncol.* **2016**, *17* (2), No. e39.
(12) The Lancet Oncology. The Lancet Oncology. Rethinking traditional Chinese medicines for cancer. *Lancet Oncol.* **2015**, *16* (15), 1439.
(13) Yu, Y.; Shen, M.; Song, Q.; Xie, J. Biological activities and pharmaceutical applications of polysaccharide from natural resources: A review. *Carbohydr. Polym.* **2018**, *183*, 91−101.
(14) Hu, Y.; Zhang, J.; Zou, L.; Fu, C.; Li, P.; Zhao, G. Chemical characterization, antioxidant, immune-regulating and anticancer activities of a novel bioactive polysaccharide from Chenopodium quinoa seeds. *Int. J. Biol. Macromol.* **2017**, *99*, 622−629.
(15) Bhat, A. A.; Gupta, G.; Alharbi, K. S.; et al. Polysaccharide-Based Nanomedicines Targeting Lung Cancer. *Pharmaceutics* **2022**, *14* (12), 2788.
(16) Wang, Y.; Qin, S.; Pen, G.; et al. Original Research: Potential ocular protection and dynamic observation of Polygonatum sibiricum polysaccharide against streptozocin-induced diabetic rats' model. *Exp. Biol. Med.* **2017**, *242* (1), 92−101.
(17) Cui, X.; Wang, S.; Cao, H.; et al. A Review: The Bioactivities and Pharmacological Applications of Polygonatum sibiricum polysaccharides. *Molecules* **2018**, *23* (5), 1170.
(18) Zeng, G. F.; Zhang, Z. Y.; Lu, L.; et al. Protective effects of Polygonatum sibiricum polysaccharide on ovariectomy-induced bone loss in rats. *J. Ethnopharmacol.* **2011**, *136* (1), 224−229.
(19) Tian, H.; Liu, Z.; Pu, Y.; Bao, Y. Immunomodulatory effects exerted by Poria Cocos polysaccharides via TLR4/TRAF6/NF-κB signaling in vitro and in vivo. *Biomed. Pharmacother.* **2019**, *112*, 108709.
(20) Sun, T.; Liu, Y.; Li, Z.; Gong, G.; Wang, Z.; Huang, L.; Zhang, H. Based on Step Alcohol Precipitation on Physicochemical Properties and Immune Activity of Polysaccharides from Wine-Processed *Polygonatum sibiricum*. *Chin. Arch. Tradit. Chin. Med.* **2023**, *41* (2), 78−84 + 263−265.
(21) Javed, J.; Yadav, S. Advanced therapeutics avenues in hepatocellular carcinoma: A novel paradigm. *Med. Oncol.* **2023**, *40* (8), 239.
(22) Yu, Y.; Shen, X.; Xiao, X.; Li, L.; Huang, Y. Butyrate Modification Promotes Intestinal Absorption and Hepatic Cancer Cells Targeting of Ferroptosis Inducer Loaded Nanoparticle for Enhanced Hepatocellular Carcinoma Therapy. *Small* **2023**, *19* (36), No. e2301149.
(23) Liu, X.; Wu, Z.; Guo, C.; et al. Hypoxia responsive nano-drug delivery system based on angelica polysaccharide for liver cancer therapy. *Drug Delivery* **2022**, *29* (1), 138−148.
(24) Singh, S. Glucose decorated gold nanoclusters: A membrane potential independent fluorescence probe for rapid identification of cancer cells expressing Glut receptors. *Colloids Surf., B* **2017**, *155*, 25−34.
(25) Bhagat, S.; Tyagi, S.; Singh, S. Monosaccharide-directed selective internalization of gold and silver nanoparticles in hepatic cancer cells. *Part. Part. Syst. Charact.* **2023**, *40* (11), 2300079.
(26) Liu, R.; Pei, Q.; Shou, T.; Zhang, W.; Hu, J.; Li, W. Apoptotic effect of green synthesized gold nanoparticles from Curcuma wenyujin extract against human renal cell carcinoma A498 cells. *Int. J. Nanomed.* **2019**, *14*, 4091−4103.
(27) Mintz, K. J.; Leblanc, R. M. The use of nanotechnology to combat liver cancer: Progress and perspectives. *Biochim. Biophys. Acta, Rev. Cancer* **2021**, *1876* (2), 188621.
(28) Bagheri, S.; Yasemi, M.; Safaie-Qamsari, E.; et al. Using gold nanoparticles in diagnosis and treatment of melanoma cancer. *Artif. Cells, Nanomed., Biotechnol.* **2018**, *46* (sup1), 462−471.
(29) Khan, M. A.; Khan, M. J. Nano-gold displayed anti-inflammatory property via NF-kB pathways by suppressing COX-2 activity. *Artif. Cells, Nanomed., Biotechnol.* **2018**, *46* (sup1), 1149−1158.
(30) Zhu, J.; Liu, Z.; Pu, Y.; Xu, J.; Zhang, S.; Bao, Y. Green synthesized gold nanoparticles from *Pseudobulbus Cremastrae seu Pleiones* show efficacy against hepatic carcinoma potentially through immunoregulation. *Drug Delivery* **2022**, *29* (1), 1983−1993.
(31) Yang, Z.; Liu, Z.; Zhu, J.; Xu, J.; Pu, Y.; Bao, Y. Green synthesis and characterization of gold nanoparticles from Pholiota adiposa and their anticancer effects on hepatic carcinoma. *Drug Delivery* **2022**, *29* (1), 997−1006.
(32) Haiss, W.; Thanh, N. T.; Aveyard, J.; Fernig, D. G. Determination of size and concentration of gold nanoparticles from UV-vis spectra. *Anal. Chem.* **2007**, *79* (11), 4215−4221.
(33) Yau, T.; Hsu, C.; Kim, T. Y.; et al. Nivolumab in advanced hepatocellular carcinoma: Sorafenib-experienced Asian cohort analysis. *J. Hepatol.* **2019**, *71* (3), 543−552.
(34) Ramzy, L.; Nasr, M.; Metwally, A. A.; Awad, G. A. S. Cancer nanotheranostics: A review of the role of conjugated ligands for overexpressed receptors. *Eur. J. Pharm. Sci.* **2017**, *104*, 273−292.
(35) Hu, J.; Huang, W.; Zhang, F.; Luo, X.; Chen, Y.; Xie, J. Variability of Volatile Compounds in the Medicinal Plant Dendrobium officinale from Different Regions. *Molecules* **2020**, *25* (21), 5046.
(36) García-Ortiz, A.; Serrador, J. M. Nitric Oxide Signaling in T Cell-Mediated Immunity. *Trends Mol. Med.* **2018**, *24* (4), 412−427.
(37) Lundberg, J. O.; Weitzberg, E. Nitric oxide signaling in health and disease. *Cell* **2022**, *185* (16), 2853−2878.
(38) Zelová, H.; Hošek, J. TNF-α signalling and inflammation: interactions between old acquaintances. *Inflammation Res.* **2013**, *62* (7), 641−651.
(39) Li, K.; Qiu, H.; Yan, J.; et al. The involvement of TNF-α and TNF-β as proinflammatory cytokines in lymphocyte-mediated adaptive immunity of Nile tilapia by initiating apoptosis. *Dev. Comp. Immunol.* **2021**, *115*, 103884.
(40) Ablasser, A.; Poeck, H.; Anz, D.; et al. Selection of molecular structure and delivery of RNA oligonucleotides to activate TLR7 versus TLR8 and to induce high amounts of IL-12p70 in primary human monocytes. *J. Immunol.* **2009**, *182* (11), 6824−6833.
(41) Kaplanov, I.; Carmi, Y.; Kornetsky, R.; et al. Blocking IL-1β reverses the immunosuppression in mouse breast cancer and synergizes with anti-PD-1 for tumor abrogation. *Proc. Natl. Acad. Sci. U. S. A.* **2019**, *116* (4), 1361−1369.
(42) Silva, J. R.; Sales, N. S.; Silva, M. O.; et al. Expression of a soluble IL-10 receptor enhances the therapeutic effects of a papillomavirus-associated antitumor vaccine in a murine model. *Cancer Immunol., Immunother.* **2019**, *68* (5), 753−763.
(43) Skubleny, D.; Lin, A.; Garg, S.; et al. Increased CD4/CD8 Lymphocyte ratio predicts favourable neoadjuvant treatment response in gastric cancer: A prospective pilot study. *World J. Gastrointest. Oncol.* **2023**, *15* (2), 303−317.
(44) Long, T.; Liu, Z.; Shang, J.; et al. Polygonatum sibiricum polysaccharides play anti-cancer effect through TLR4-MAPK/NF-κB signaling pathways. *Int. J. Biol. Macromol.* **2018**, *111* (111), 813−821.
(45) Zhao, W.; Li, J.; Zhong, C.; Zhang, X.; Bao, Y. Green synthesis of gold nanoparticles from Dendrobium officinale and its anticancer effect on liver cancer. *Drug Delivery* **2021**, *28* (1), 985−994.

https://doi.org/10.1021/acsomega.4c01025
ACS Omega 2024, 9, 21144−21151